*Agreement INGV-DPC 2007-2009*

# Project S 1: Analysis of the seismic potential in Italy for the evaluation of the seismic hazard

*Responsible: Salvatore Barba (INGV Roma 1) and Carlo Doglioni (Roma University of the "La Sapienza")*

http://groups.google.com/group/INGV-DPC-2007-S1
(restricted access)

Deliverable 2 # A3.13.8

## Delimitation of Near-fields boundaries (Final Report)

*June 10, 2010*

*prepared by UR 3.13*

*Zonno Gaetano[1], Musacchio Gemma[1], Meroni Fabrizio[1], Basili Roberto[2], Imperatori Walter[3] and Mai P. Martin[3,*]*

*[1] Istituto Nazionale di Geofisica e Vulcanologia, Sezione di Milano-Pavia, Milano*

*[2] Istituto Nazionale di Geofisica e Vulcanologia, Sezione di Roma 1, Roma*

*[3] Institute of Geophysic, ETH Zurich, Switzerland*

*(*)New affiliation (as of June 1, 2009) King Abdullah University of Science & Technology (KAUST), Division of Physical Sciences & Engineering (Thuwal, Saudi Arabia)*

# 1. Description of the Deliverable

## 1.1 Introduction

As outlined in the report to Phase 1 (April 30, 2009), we examine possibilities to delineate the boundaries between near-field and far-field radiation of seismic waves. Near-field (NF), intermediate-field (IF) and far-field (FF) terms represent different properties of the seismic wave-field: the near-source motions are sensitive to the spatio-temporal details of the rupture process, while far-field terms tend to carry the overall signature of the rupture. Due to the longer propagation path of far-field waves through complex Earth structure, their waveform properties also depend more strongly on media properties (scattering; intrinsic attenuation), than it is the case for the NF-wavefield. However, from a theoretical view point, there is no strict boundary that marks the NF and FF-region, since there is no distance at which the NF terms can be completely ignored (Aki & Richards, 2002; Wu and Ben-Menahem, 1985; Ichinose et al, 2000; Mai and Beroza, 2003). Note also that, generally speaking, the NF- and FF-terms are frequency dependent in that FF-terms contain higher frequencies than NF-terms.

Nevertheless, for ground-motion prediction/simulation it may be beneficial to approximately delineate the region in which near-field terms need to be included for accurate shaking-level estimation (and beyond which it is sufficient to only consider the dominating far-field radiation). Many efficient approaches have been devised to simulate ground motion in the far-field regime (see Mai, 2009, and references therein), neglecting near-field effects and also to a large extent the details of the rupture process. However, for complete and fully realistic ground-motion simulations, computationally more expensive calculations are needed that include near-field radiation and detailed earthquake source descriptions. Thus, depending on the particular engineering application and seismic design criteria, it may be sufficient to perform approximate high-frequency far-field ground-motion simulation instead of carrying out expensive full wavefield computations that contain all NF, IF, and FF-terms. The goal of this study is to help address the question if this near-field/far-field boundary can in fact be adequately be defined.

In the following we will first summarize the key aspects of seismic-source theory that address near-field and far-field seismic radiation. We then describe our simulation strategy for examining the properties of NF- and FF-seismic waves from extended sources. The original project description includes a theoretical/analytical study on this issue, however, we decided to focus on the numerical aspects of this work to gain insight into the NF/FF properties from to potentially derive an application-oriented empirical relations. Descriptions and analysis of our simulation results and a summary section conclude the report.

## 1.2 Review of source theory regarding near-field / far-field radiation

The time-dependent ground displacement $u_k(t)$ at the observer location $k$ due to a seismic source can be described by the convolution of a source term $s(t)$ with a wave-propagation term $g_k(t)$, potentially augmented with a site-effect contribution $l_k(t)$ (where $\underline{x}$ is the vector denoting the spatial position of the observer location):

$$u_k(\underline{x},t) = s(t) * g_k(t) * l_k(t) \tag{1}$$

There are numerous ways to parameterize this equation and numerically solve it for the purpose of ground-motion calculation, depending on the particular problem. In case only the

far-field displacements due a to point-source are desired, the source term can be replaced with, for instance, the moment-tensor and the wave-propagation term with the far-field Green's function derivatives.

However, ground-motions that contribute to the seismic hazard at a given site generally cannot be described by a simple equation involving the moment-tensor point-source representation. In this case, finite-fault effects are likely to become important, while also the effects of the near-field terms in the Green's function formulation of the radiated elastic energy need to be considered. The general expression for internal dislocation sources is given in a representation theorem of the following form:

$$u_k(\underline{x},t) = \int_{-\infty}^{\infty} d\tau \iint_{\Sigma} \left[u_i(\xi,\tau)\right] \cdot c_{ijpq} \cdot \nu_j \cdot \frac{\partial}{\partial \xi_q} G_{np}(\underline{x},t-\tau;\xi,0) d\Sigma \qquad (2)$$

In Eq. [2], the space-time evolution of the kinematic source process is given by $u_i(\xi,\tau)$, $c_{ijpq}$ denotes the elasticity tensor, $\nu_j$ the fault normal vector, and the last part describes the Green's function derivative. Inserting into [2] the elasto-dynamic Green's functions and a double-couple source description reveals that:

- Near-field waves are composed of both P- and S-wave, depend on the temporal slip-evolution on the fault plane, and decay as $1/r^3$ with distance $r$;
- Intermediate-field exist for P- and S-waves separately, their amplitude and properties depend on the slip function, and their distance decays goes as $1/r^2$
- Far-field P- and S-waves depend on the slip-rate function and decay as $1/r$.

Thus, near-field (NF), intermediate-field (IF) and far-field (FF) terms represent different properties of the wave-field: the near-source motions are more sensitive to the spatio-temporal details of the rupture process, while far-field terms carry the overall signature of the rupture encoded into the moment-rate function. On the other end, the high-frequency far-field motions often exhibit peak ground acceleration (*PGA*) within the resonance frequency of buildings, and hence are of great interest for engineering purposes.

In this context it is of interest to be able to define the (approximate) region in which NF-radiation needs to be included, and where FF-waves dominate. Ground motion simulations codes have been developed to compute either the NF or FF wave-field, with computational costs increasing rapidly if full-wave field simulations are needed. Fully broadband (i.e., including the complete frequency domain of engineering interest) simulation techniques using a single methodology are not feasible due to computational limitations, and hence hybrid approaches are considered (e.g. Mai & Beroza, 2003; Graves and Pitarka, 2004; Mai et al., 2010; Mena et al, 2010).

An insightful, yet simplified, study has been carried out by Ichinose et al. (2000) to address the importance of near-field and far-field radiation in layered media for point-source excitation. Their conclusion states that "*the importance of near- and intermediate-field terms for the synthesis of complete waveforms can be significant out to regional distances (330 km) at very long periods*" (Ichinose et al., 2000). More specifically, near-field and far-field radiation needs to be treated frequency dependent, in that the far-field terms dominate already at short distances for high frequencies, while for low frequencies the near-field terms may be important to large distances. This statement can be recast into a dimensionless scalar, valid for a homogeneous half-space (e.g. Madariaga, 2009), that outlines the far-field condition

$$\frac{\omega \cdot R}{c} ? \; 1. \tag{3}$$

In Eq. [3], $\omega$ is angular frequency, $R$ is hypocentral distance, and $c$ the corresponding wave speed. Rewriting [3] in terms of wavelengths yields $R/\lambda >> 1$, where $\lambda = 2\pi c/\omega$. We see once more that the far-field condition depends on the characteristic frequency (or wavelength) of seismic radiation: depending on the frequency content of the signal, we may be in the far-field for high-frequencies at a particular observer location, while for the low frequency wave field the same location experiences near-field effects. In the limit, for zero-frequency waves, i.e. the static displacement, all points on the Earth are, theoretically, in the near-field domain. However, for many practical purposes, a standard statement is that for frequencies above 1Hz, the far-field condition is fulfilled for distances larger than 10 km (Madariaga, 2009).

Ichinose et al (2000) interpret the ratio in Eq. [3] slightly differently, stating that the near-field term is significant for all $R$ within a small fraction of a wavelength, $g$. Using numerical simulations they examine whether Eq. [3] holds for layered media also, and conjectured that $g$ in the range 0.6 – 1.0 provides an adequate approximation: once the seismic wave has propagated about one wavelength away from the hypocenter, the far-field terms dominate. Eq. [3] can be rewritten to estimate the frequency at which far-field and complete solution converge: $f_{NF} = g\, c\, /R$.

However, the preceding discussions related to Eq. [3] do not address the case of extended-fault ruptures in which the main seismic moment release may be far from the hypocenter location, and where directivity effects, variations in rupture speed, heterogeneous slip distributions, and variable rise times on the fault lead to large spatial variability in the seismic motions. One therefore could expect that a more complete characterization for the far-field condition for seismic radiation would invoke some dependency on source parameters as well. In this study, we make a first step in this direction by means of numerical simulations.

### 1.3 Simulation Strategy

To study the importance of near-field and far-field contributions in the seismically radiated wavefield, we perform numerical simulations for a number source-model realizations, using two different finite-fault ground-motion simulation techniques that account for rupture model complexity. Both numerical codes consider 1D layered velocity structures. We compute high-frequency (up to ~10 Hz) far-field (FF) radiation using the ISOSYN package (Spudich & Xu, 2003), for arbitrarily complex source-rupture models. This code implements the isochrone theory (Spudich & Frazer, 1984; Bernard & Madariaga, 1984). Low frequency ($f \leq 2$ Hz) complete seismograms, containing additionally all NF and IF terms, are computed using the COMPSYN package (Spudich & Xu, 2003), a discrete-wavenumber / finite-element code.

The COMPSYN code for the low-frequency full-wavefield simulations has been widely tested and applied, and allows specifying arbitrarily complex rupture models. For chosen velocity-density model and source-receiver geometry, the tractions on the fault are pre-computed (a computationally expensive step), while the subsequent convolution of the tractions with the rupture model is efficiently done in the frequency domain. The ISOSYN-code provides a very efficient, yet approximate, high frequency (ray theoretical) ground-motion simulation technique, considering only the direct P- and S-waves, but handling the

exact same source models as generated for the COMPSYN simulations. The ISOSYN- high-frequency computations are fully deterministic, i.e. no scattering or complicated quasi-random wave-propagation at high frequencies is included.

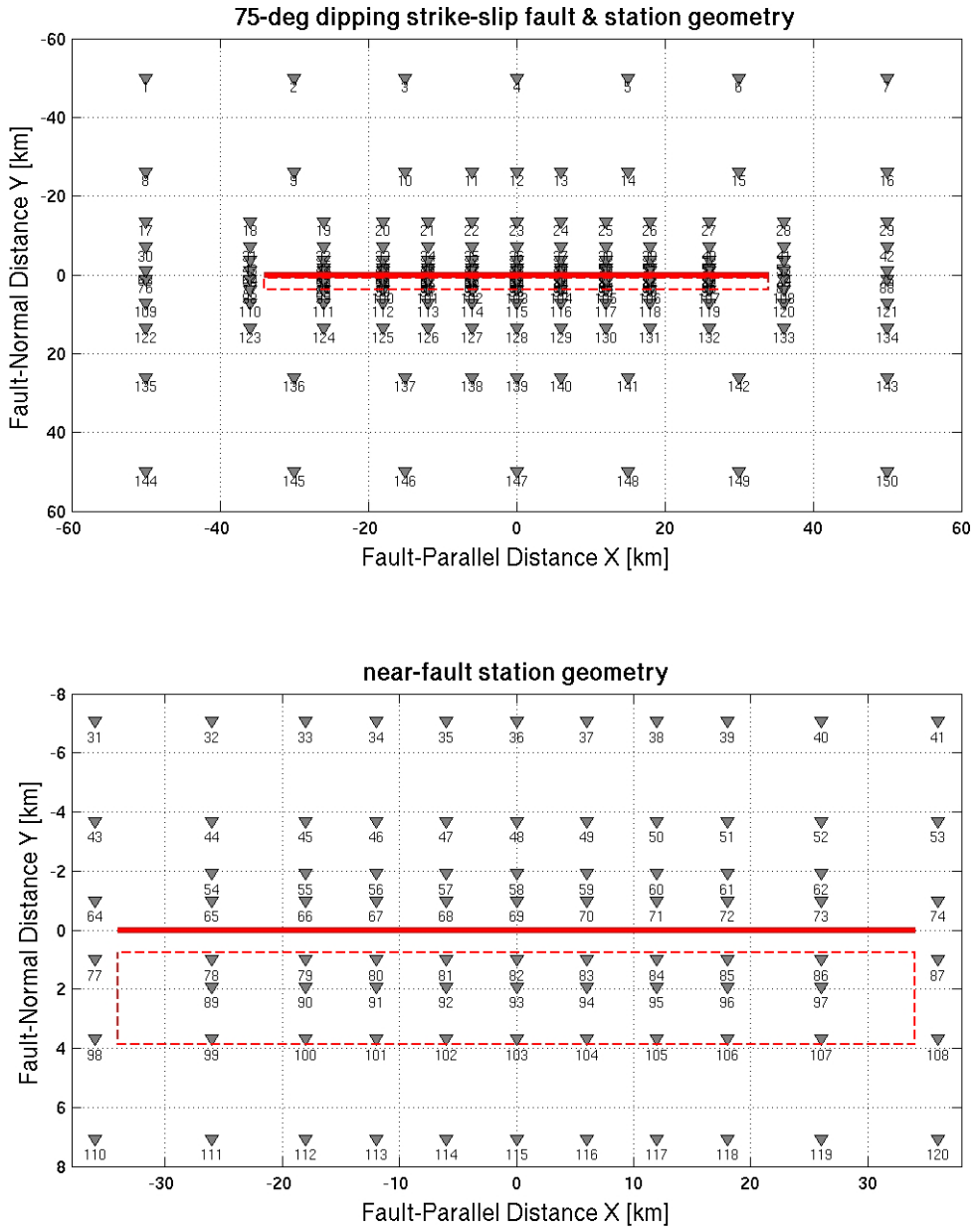


Figure 1. Station geometry used in this study. 150 sites are located at approximately regular inter-station spacing in fault-parallel (X) direction, approximately logarithmically spaced in fault-normal (Y) direction. The sold red line marks the surface-projection of the upper edge of the fault plane, the dotted line shows the projection of the 75°-dipping fault. Top: entire simulation domain; bottom: near-fault region only.

While our initial set of simulations (see Report to Phase 1, April 30, 2009) used simplified source models (uniform slip, uniform rise time, and constant rupture speed) to obtain first-order estimates on NF/FF radiation effects, we here refine our work by using a variety of faulting styles, fault geometries, and different realizations of heterogeneous slip on the fault.

We also modified the station distribution (Figure 1) to fully include footwall and hanging wall effects as well as capturing a larger distance range. The velocity-density model (Figure 2) has been changed to roughly correspond to the structural model for the Colfiorito region, with slight modification to suppress strong surface-wave contributions, which have been found to dominate over NF/FF effects (see Report to Phase 1, April 30, 2009). The different source geometries and source parameters are listed in Table 1.

For the selected source-site geometry (Figure 1), the chosen velocity-density structures (gradient and layer model, Figure 2) and the source-model sizes (Table 1), we pre-compute the tractions on the fault for the full-wavefield COMPSYN simulations. Given the maximum resolving frequency of f = 2 Hz, this results in traction-files with total storage space of 91Gb for the layered velocity model; the gradient model results in 83Gb required storage. Using these traction files, we then compute the ground-motions for the rupture models shown in Figure 3, resulting in 150 x 3 x 10 x 2 = 9'000 time series (station x components x source models x velocity models). For the isochrone synthetics, we only use the gradient velocity model (since the ISOCHRONE code cannot handle triplications). Time series contain 2048 points, sampled at dt = 0.03 sec, resulting in 61.44 sec long synthetic seismograms.

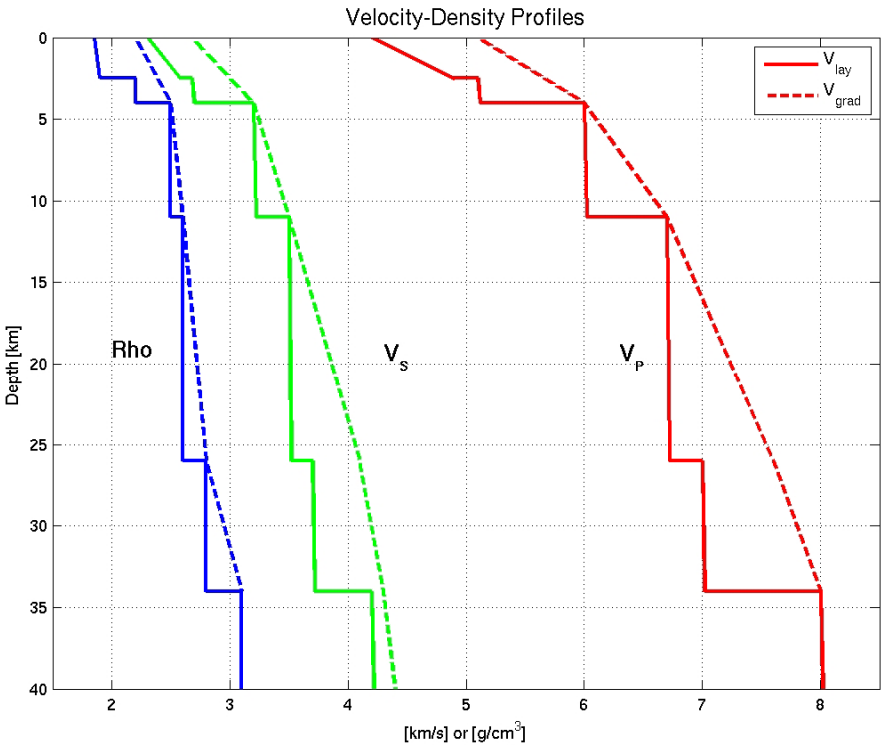


Figure 2. Velocity-density model used for near-field & far-field ground-motion simulation. Model $V_{lay}$ consists of several layers with strong discontinuities; model $V_{grad}$ is a linear-gradient model anchored to $V_{lay}$, and avoids travel-time triplications (dashed line).

| Name | Faulting Style | Dip [deg] | Size [LxW km] | Rise time [s] |
|---|---|---|---|---|
| DS25Mod3 | thrust faulting | 25 | 50 x 23 | 1.4 |
| DS25Mod5 | thrust faulting | 25 | 50 x 23 | 1.4 |
| DS25Mod6 | thrust faulting | 25 | 50 x 23 | 1.4 |

| | | | | |
|---|---|---|---|---|
| DS45Mod3 | normal faulting | 45 | 50 x 16 | 1.4 |
| DS75Mod5 | normal faulting | 75 | 50 x 11 | 1.4 |
| TF71Mod1 | RL strike slip | 75 | 69 x 12 | 1.4 |
| TF71Mod2 | RL strike slip | 75 | 69 x 12 | 1.4 |
| TF71Mod4 | RL strike slip | 75 | 69 x 12 | 1.4 |
| TF71Mod6 | RL strike slip | 75 | 69 x 12 | 1.4 |
| TF71Mod7 | RL strike slip | 75 | 69 x 12 | 1.4 |

Table 1. Specification of rupture models used in this study.

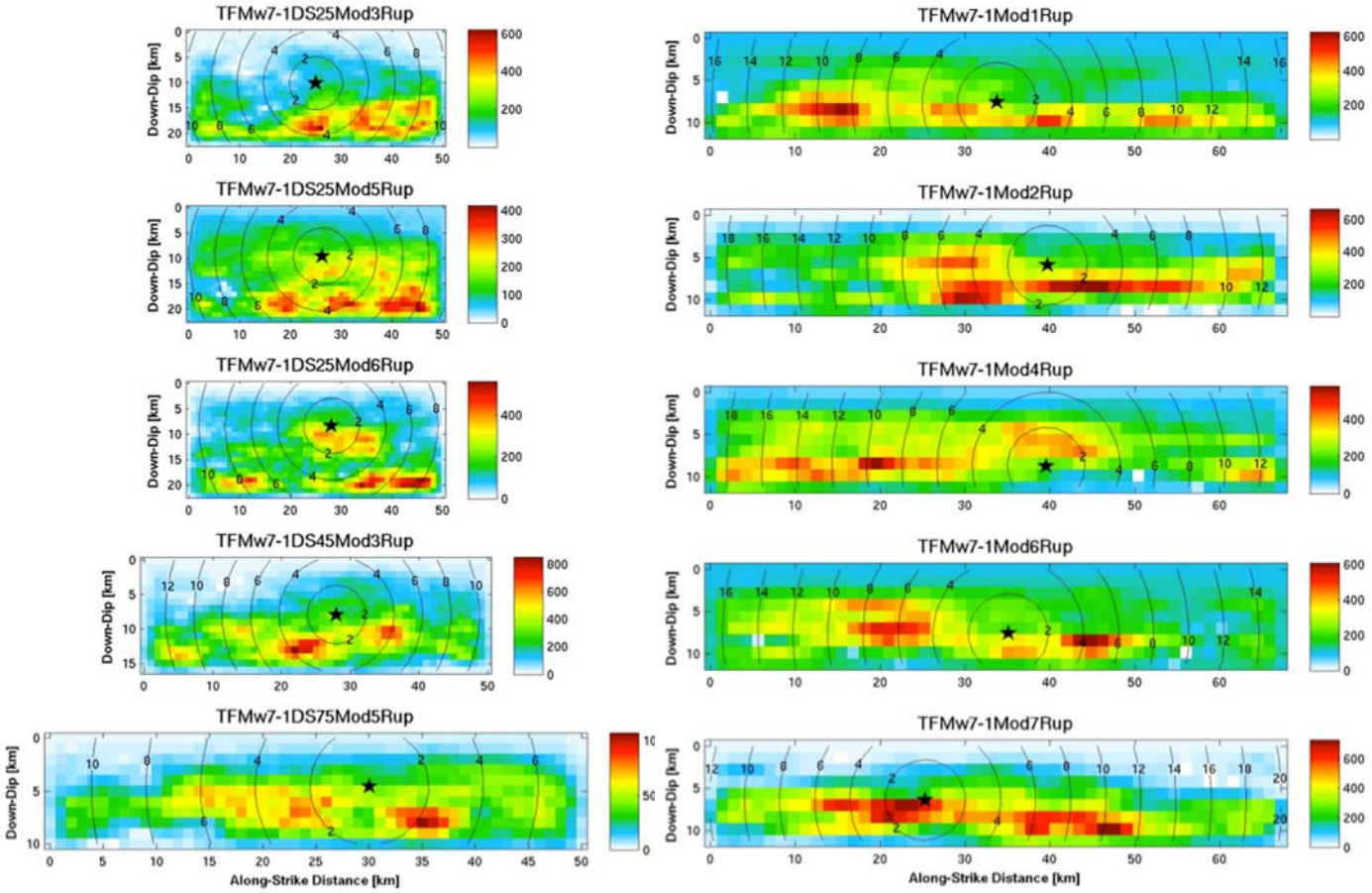


Figure 3. Dip-slip rupture models (left) and strike-slip rupture models (right). The color indicate the slip (in cm) on the fault plane, the star marks the hypocenter. White contour lines show the rupture propagation over the fault plane at 2-sec intervals.

As indicated in Table 1, rise time for all rupture models was chosen to be a uniform1.4 sec over the fault plane, consistent with scaling relations of Somerville et al. (1999). We use a simple boxcar slip-velocity function of this width to compute both COMPSYN and ISOCHRONE synthetics. Rupture speed is fixed at 80% of the local shear-wave speed, and thus leads to rupture propagation at 2.2-2.7 km/s, depending on depth-extent of the rupture

model. In our simulations, we put the upper-edge of the fault plane at a uniform Ztop = 1 km. While this is a simplification compared to the DISS database (which lists depth of 10 km for certain steeply dipping typical faults), it facilitates our comparisons and presents a type of "worst-case scenario" in terms of near-fault radiation. For the deeper events, near-field terms are expected to be even less important; therefore we focus on shallower ruptures for studying the near-field effects.

### 1.4 Approximate model for near-field importance

Using Equation [3] and the station geometry for our simulation (Figure 1), we compute a first-order approximation on the distance range where near-field effects are important (Figure 4). Alternatively, the relations can be interpreted in terms of the frequency at which the near-field and far-filed terms converge. We assume an S-wave speed of 3.4 km/s, appropriate for the selected velocity model at the depth of the hypocenter. However, it is important to note that the model of Eq. [3] is valid for point-source radiation. The graphs in Figure 4 thus may only serve as a reference base case against which to compare our more detailed analysis.

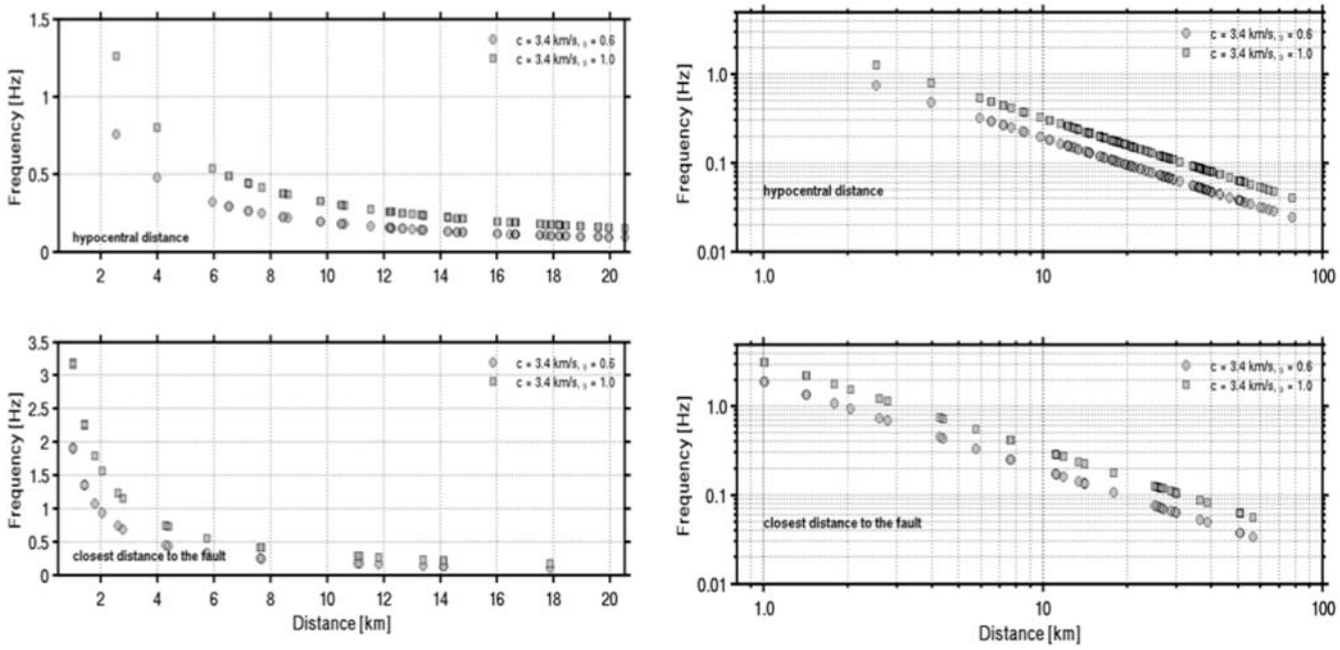


Figure 4. Importance of near-field effects, according to Eq. [3] (Ichinose et al., 2000) for typical distance measures in our study (top panels: hypocentral distance; bottom panels: closest distance to the fault). The left two graphs show the near-source range (0 – 20 km) on a linear-linear scale, the right panels depict the entire distance range of interest on a log-log-scale.

Based on the calculations shown in Figure 4, we find that this simple model predicts that at 6 km distance from the hypocenter (or closest distance to the fault), near-field terms are important for frequencies up to ~0.5 Hz. At 10 km distance this frequency drops to ~0.2 Hz, while at very near-source sites ($R \leq 2$ km), near-field effects may be important even in the 2-3 Hz range. However, this model assumes a homogeneous half-space and point-source radiation, and hence cannot be taken literally when considering complex ruptures embedded in layered or even 3D Earth structure. Moreover, this model does not consider the different

components of motion – fault-normal, fault-parallel, vertical – onto which that radiated seismic energy is partitioned, depending on the faulting style.

Starting with Figure 4, we analyze our simulations with respect to the distance/frequency range at which near-field appear to be important. We do so by including engineering-type ground-motion measures, spectral acceleration $SA_T$, which is relevant for seismic hazard and earthquake-engineering applications.

### 1.5 Examples of near-field / far-field motions

Figures 5 and 6 display fault-normal and fault-parallel seismogram, and respective response spectra, for two rupture models (DS45Mod3 and DS75Mod5), considering a fault-normal array of 8 near-fault stations (see Figure 1 for location). Red traces mark full-wavefield COMPSYN synthetics that include near-field contributions, blue traces denote ray-theory ISOCHRONE synthetics. For reference, the (approximate) P- and S-wave arrival times are marked by vertical dotted lines (arrival times are computed with a 3D ray-tracing code; Hole, 1992). Since the near-field terms consist of both P- and S-waves, they arrive between the primary P- and S-wave arrivals. Moreover, they depend on the integral of the moment-release function, and hence exhibit often a characteristic ramp-like appearance in velocity seismograms. In Figure 5 and 6, some clear examples of the near-field term are marked with green circles

To facilitate the comparison of the waveforms in Figure 5 and 6, we normalize each seismogram to unit amplitude; corresponding response spectra are computed for normalized waveforms. Examining these near-field pulses and their spectral response, we note that they may not be immediately visible on each component of motion, and they vary in strength. In fact, the relative strength of the near-field ramp seems to be stronger for stations at larger distance, which is probably an effect of the very strong single velocity pulse seen on the very near-source sites. This velocity pulse masks the near-field ramp due to its high amplitude. Note also that there are clear differences in the character of the near-field pulse for the steeply dipping rupture (DS75Mod5, Figure 5) and the more shallowly dipping event (DS45Mod3), although both share a normal-faulting source mechanism.

Aside from their expression in the seismic waveforms, the near-field terms also leave a signature on the response spectra. Note that the COMPSYN synthetics (blue) are valid only in a frequency range of 0 – 2 Hz. We thus low-pass the ISOSYN synthetics (red) also at 2 Hz (which introduces occasionally a low-frequency ramp at the onset of the primary S-wave that resembles the near-field pulse). The response spectra should therefore only be considered for periods above 0.5 sec. Nevertheless, we see distinctly different spectral values $SA_T$ between the two sets of synthetics, over a period range from roughly 1 – 10 secs, suggesting that the near-field terms are important of a wide range of distances and a wide range of frequencies relevant for earthquake engineering applications.

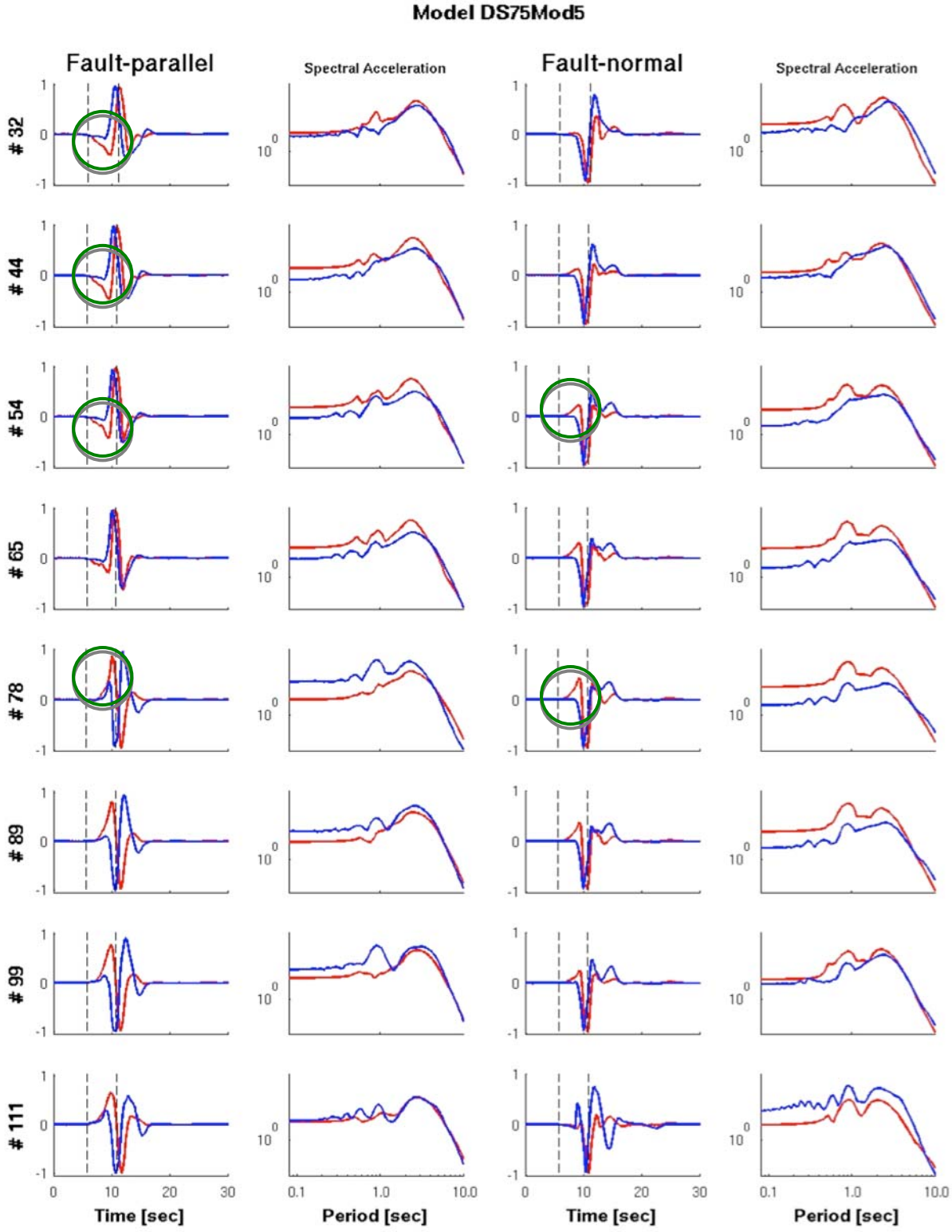


Figure 5. Fault-normal and fault-parallel seismogram, and respective response spectra, for rupture models DS75Mod5 on a fault-normal array of 8 near-fault stations. Red traces mark full-wavefield synthetics that include near-field contributions, blue traces denote ray-theory synthetics. (Approximate) P- and S-wave arrival times are marked by vertical dotted lines. Note that a mild low-pass filter applied to the ISOCHRONE synthetics (blue) introduces occasionally a ramp at the S-wave arrival that resembles the near-field pulse. Each seismic trace is normalized to unit amplitude to facilitate their comparison; response spectra are computed for the normalized waveforms.

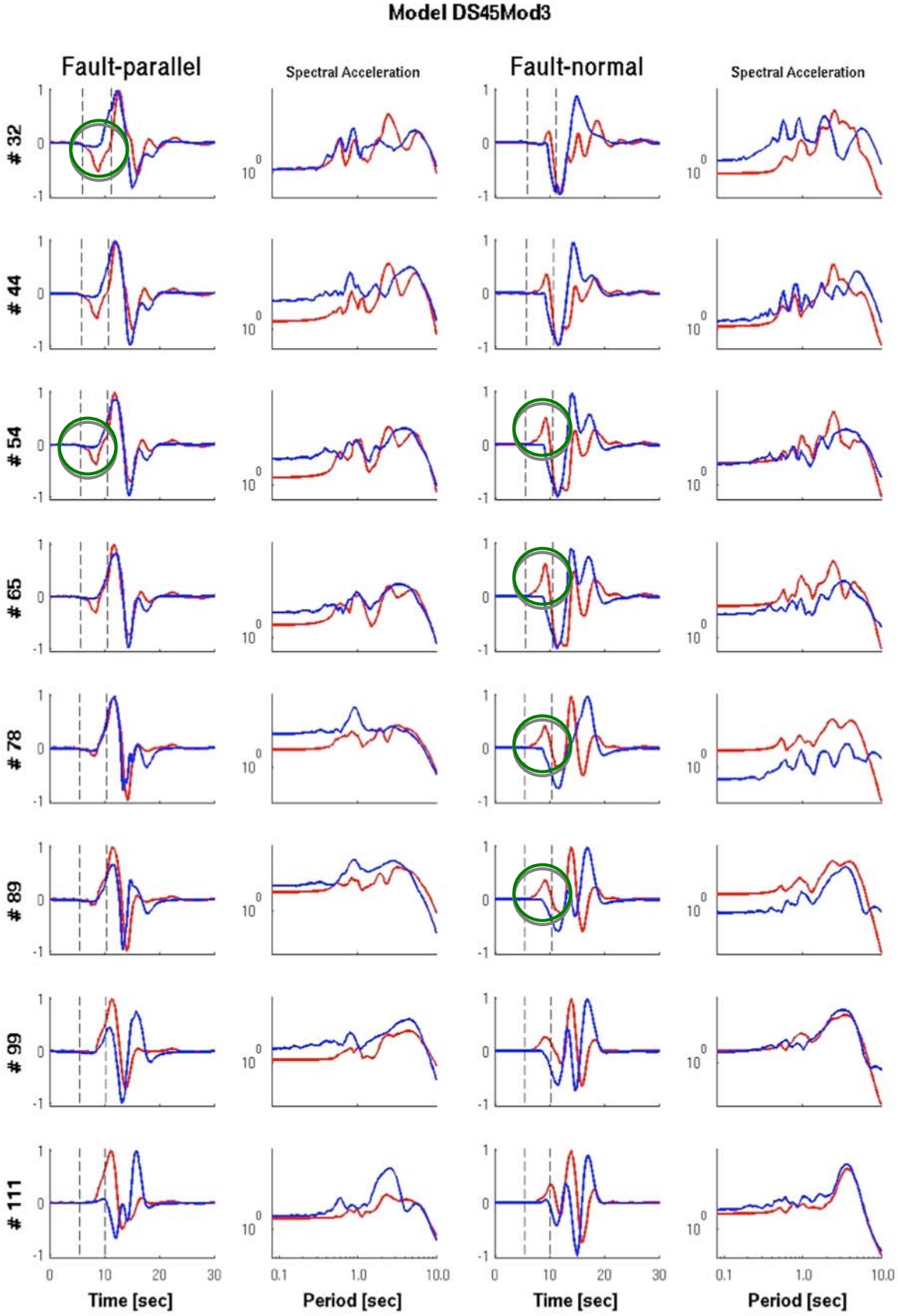


Figure 6. Same as Figure 5, for rupture models DS45Mod3.

## 1.6 Shake maps to identify near-field effects

To examine the properties and distance decay of near-field effects we plot Shake maps for COMPSYN synthetics and ISOSYN synthetics separately, for all three components of motion (fault-normal, fault-parallel, vertical) and for different ground-motion parameters (PGV, $SA_T$ for T = [1 2 3 5] sec). These maps serve as a preliminary way to quantify the importance range. Figure 7 below serves as an example to illustrate he generic differences we see between the full wavefield (COMPSYN, top), and ray-theory far-field (ISOCHRONE, bottom) ground motion.

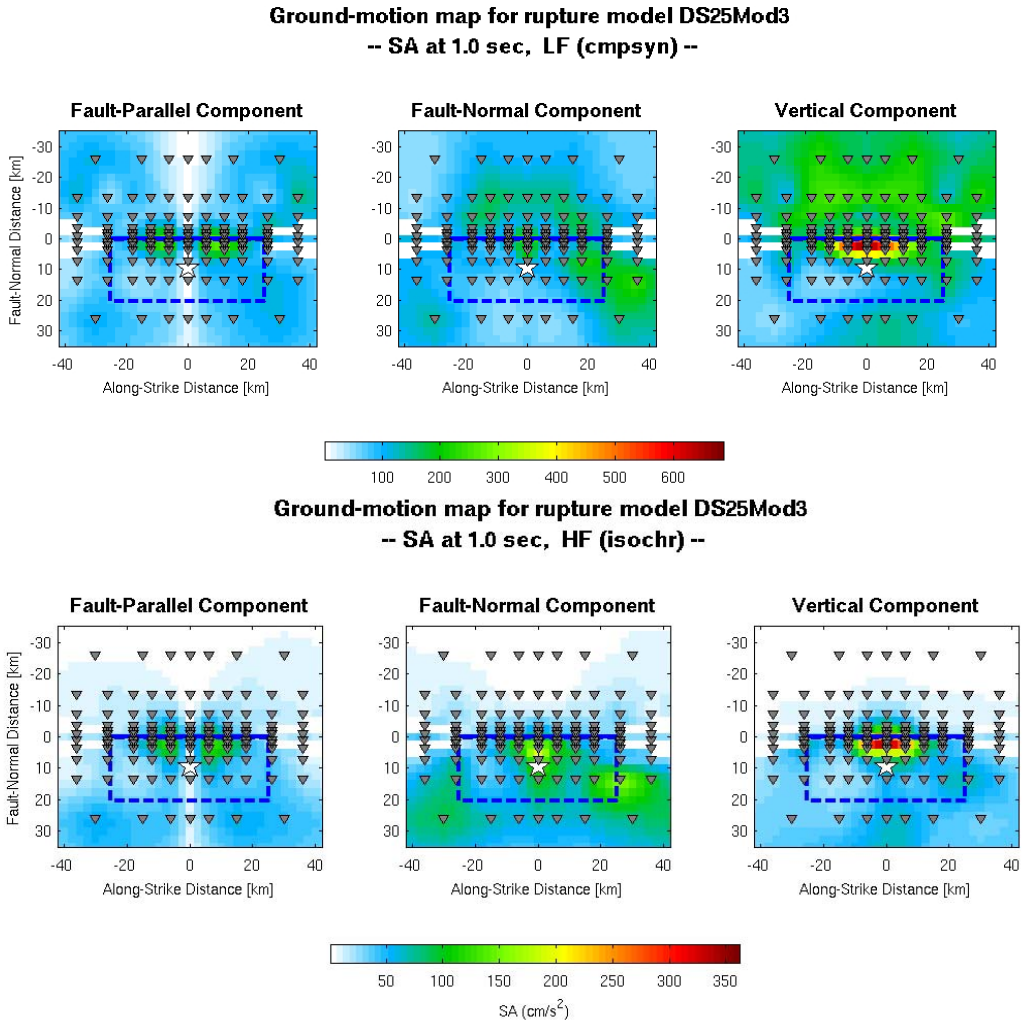


Figure 7. Shake maps for thrust-faulting scenario event DS25Mod3, showing spectral acceleration $SA_T$ at T = 1s for full-wavefield (COMPSYN, top) and ray-theory far-field (ISOCHRONE, bottom), for the fault-parallel (left column), fault-normal (center column) and vertical component of motion (right column). The blue lines indicated the surface projection of the fault plane, the star marks the epicenter; triangles are the site locations used for the simulation. The fine-gridded map is obtained through bilinear interpolation from the site motions.

As can be appreciated in Figure 7, the general distribution of shaking intensities (here measured as spectral acceleration at T = 1sec) are similar for the ISOCHRONE and COMPSYN synthetics, while however the absolute values are larger for the full wave-field simulations. However, for this thrust-faulting scenario, we notice that the ray-theory seismograms show very little shaking on the footwall (upper half of the shake map) while the full-wavefield synthetics exhibit significant shaking on the fault-normal and in particular the vertical component. This pattern of strong difference on the footwall, and in the vertical and fault-normal component, is also given at different spectral periods and for the PGV, as shown in Figure 8.

We perform a similar analysis for the 45°-dipping normal-faulting scenario (DS45Mod3, Figure 9), the 75°-dipping normal-faulting scenario (DS75Mod5, Figure 10), and the 75°-dipping strike-slip scenario (Mod1, Figure 11). We observe that the general pattern between different scenarios for a given faulting style (and with that geometry in our simulation set up) does not change much, and only shows local variations due the slip distribution on the fault plane.

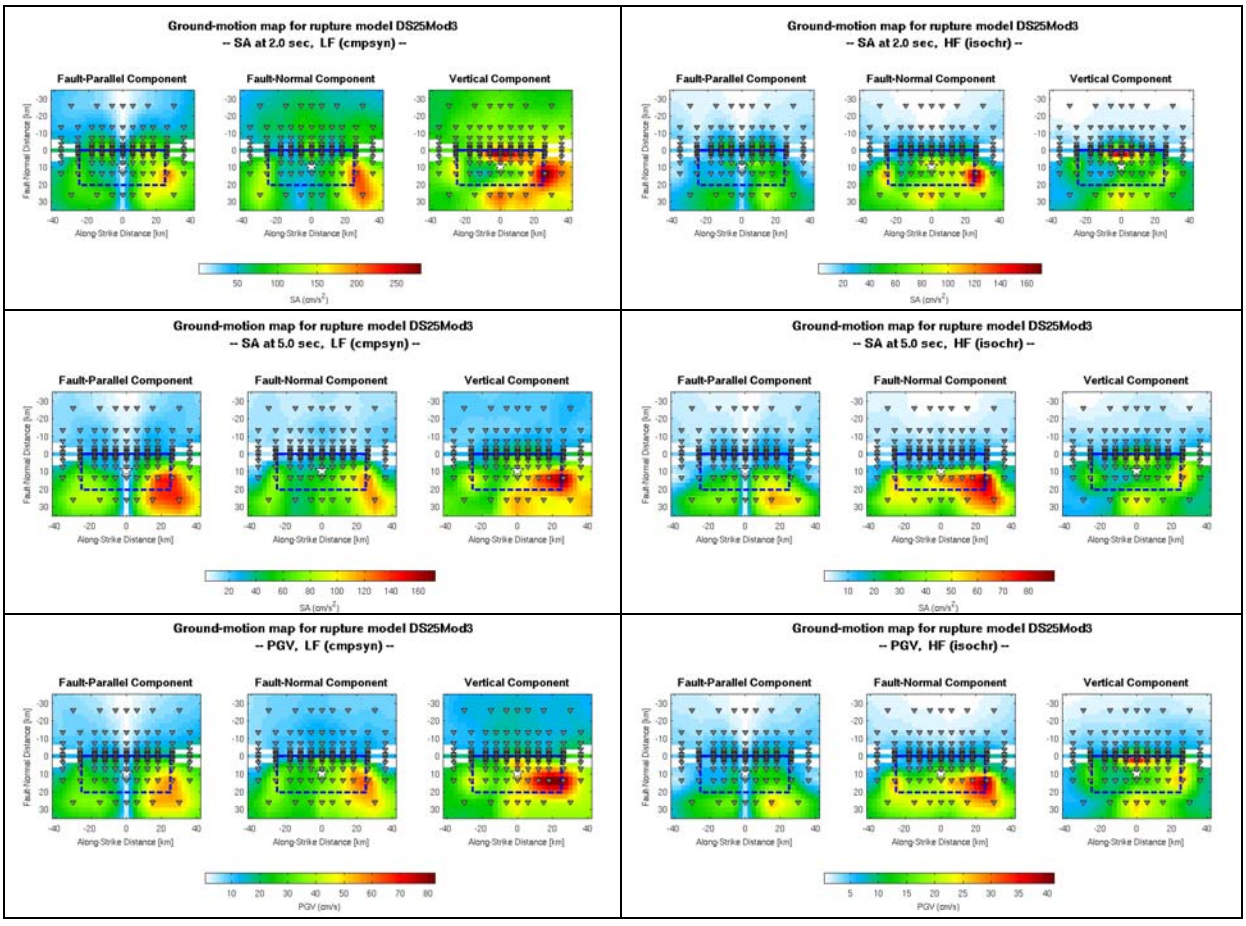


Figure 8. Shake maps for 25° dipping thrust-faulting scenario event DS25Mod3 for T = 2sec (top row), T = 5 sec (center row) and PGV (bottom row), for full-wave field (left column) and far-field (right column) synthetics. For details see Figure 7. Note the similarities in the overall shaking pattern between the two sets of synthetics, but also the differences in the details (particularly in the vertical component and for the footwall stations) due to near-field effects.

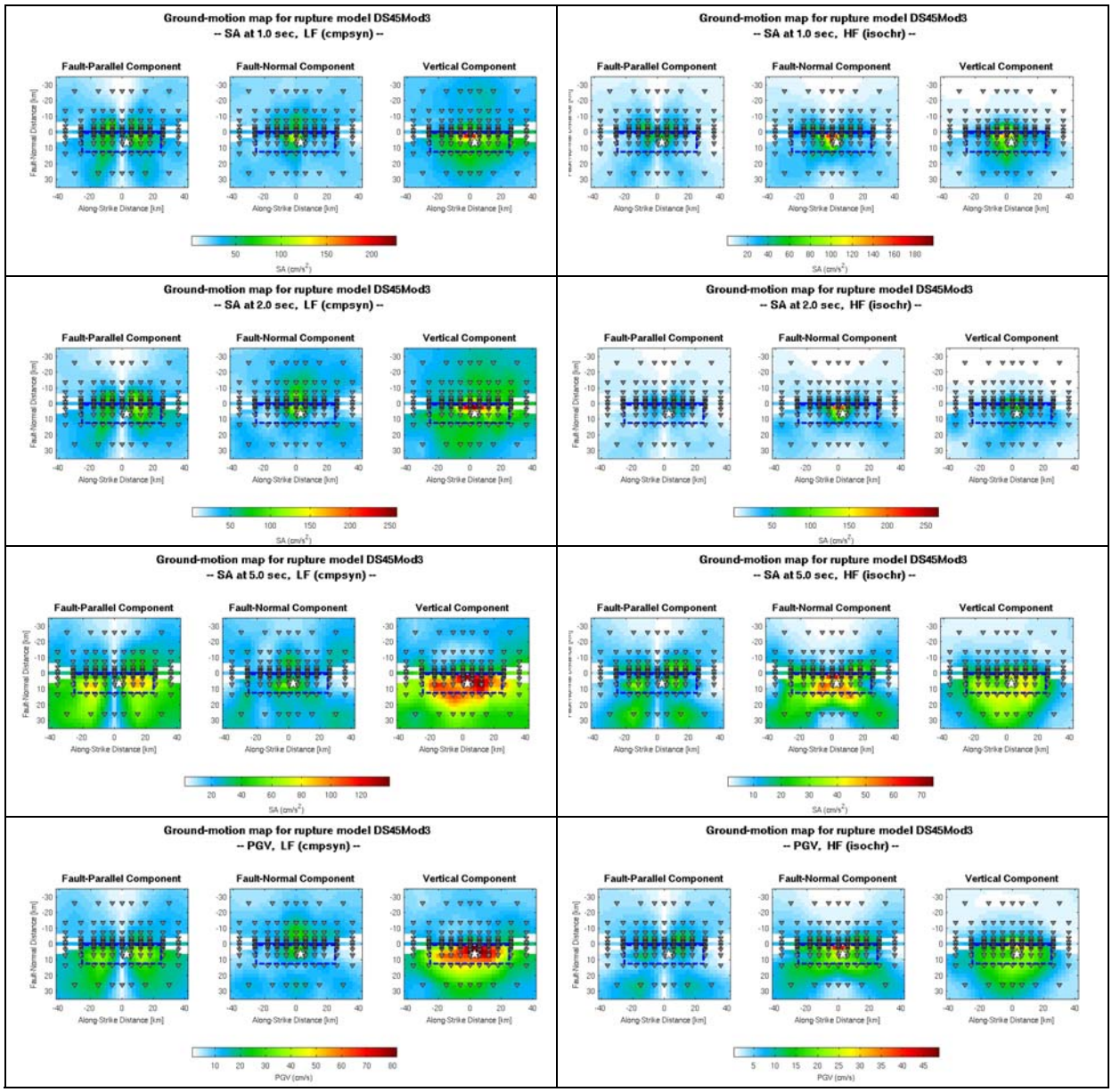


Figure 9. Shake maps for 45° dipping normal-faulting scenario event DS45Mod3 for T = 1sec (1st row), T = 2sec (2nd row), T = 5 sec (3rd row) and PGV (bottom row), for full-wave field (left column) and far-field (right column) synthetics. For details see Figure 7. Note the similarities in the overall shaking pattern between the two sets of synthetics, but also the differences in the details (particularly in the vertical component and for the footwall stations) due to near-field effects.

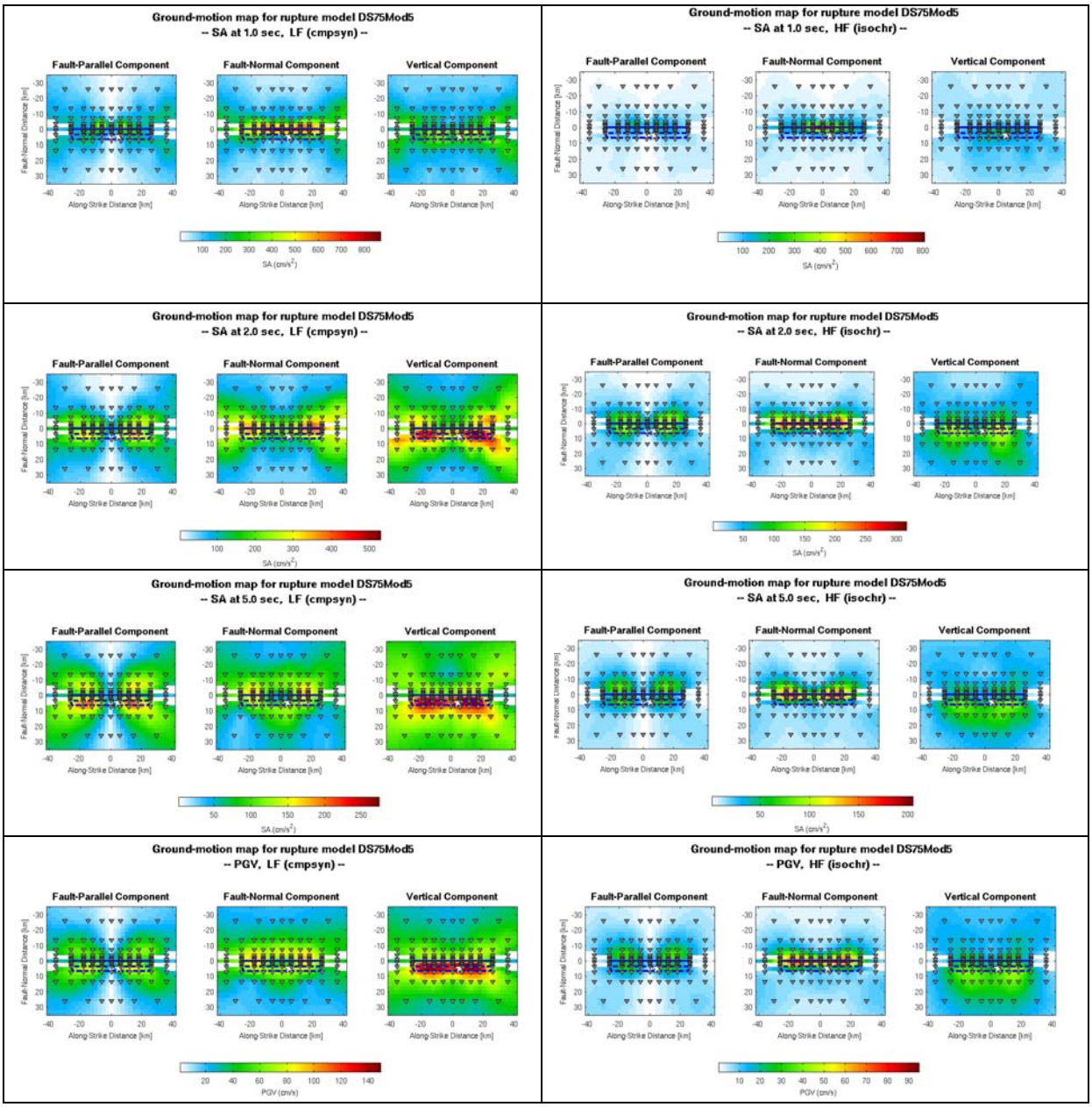


Figure 10. Shake maps for 75° dipping normal-faulting scenario event DS75Mod5 for T = 1sec (1st row), T = 2sec (2nd row), T = 5 sec (3rd row) and PGV (bottom row), for full-wave field (left column) and far-field (right column) synthetics. For details see Figure 7. Note the similarities in the overall shaking pattern between the two sets of synthetics, but also the differences in the details (particularly in the vertical component and for the footwall stations) due to near-field effects.

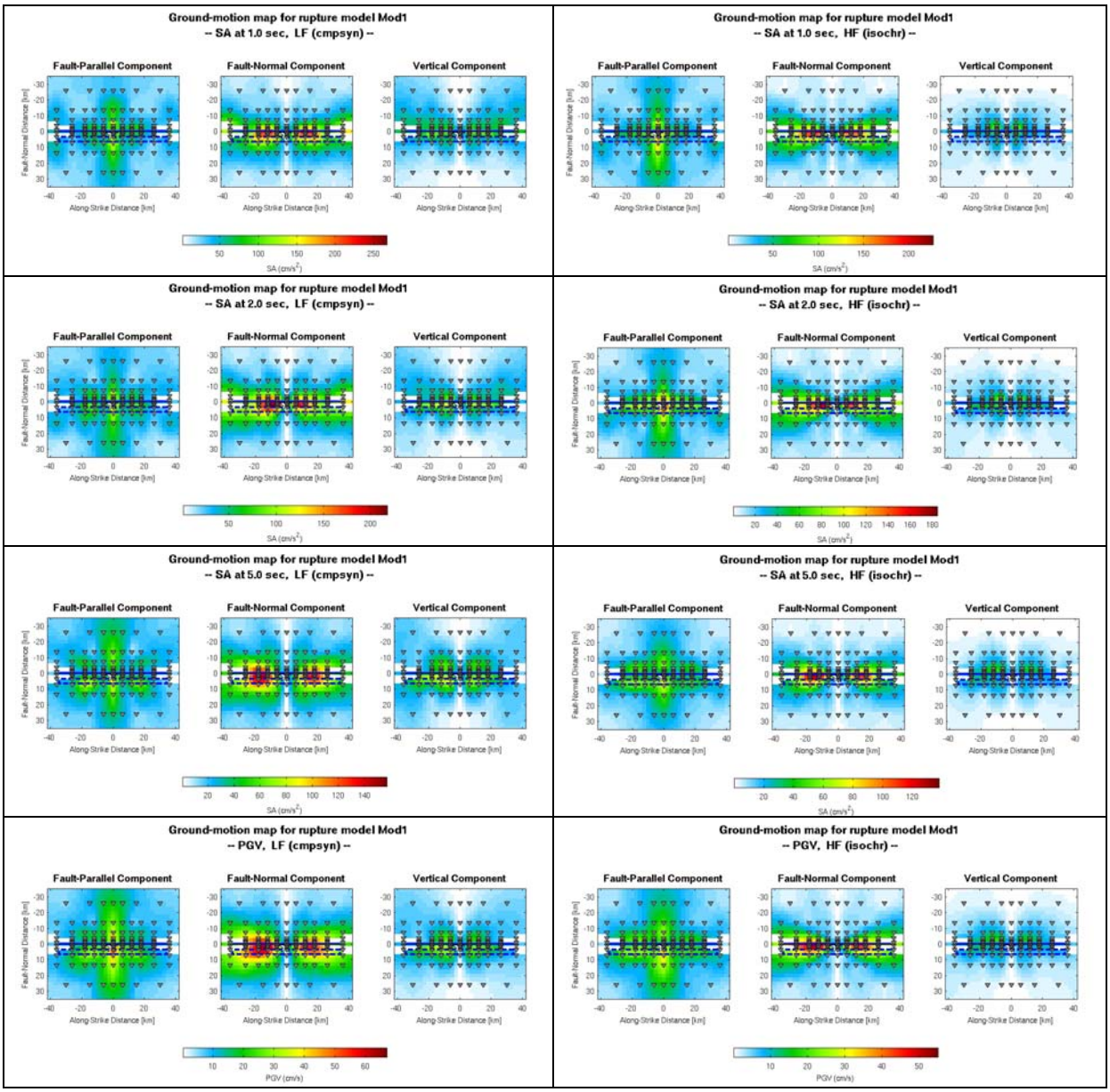


Figure 11. Shake maps for 75° dipping strike-faulting scenario event Mod1 for T = 1sec (1st row), T = 2sec (2nd row), T = 5 sec (3rd row) and PGV (bottom row), for full-wave field (left column) and far-field (right column) synthetics. For details see Figure 7. Note the similarities in the overall shaking pattern between the two sets of synthetics, but also the differences in the details (particularly in the vertical component and for the footwall stations) due to near-field effects.

## 1.7 Summary on near-field / far-field seismic radiation effects

Analyzing our suite of ground-motion simulations for 150 sites in the distance range of ±50 km from a $M_w$ 7.1 scenario event, occurring on a 25°-dipping thrust-fault, a 45°-dipping or 75°-dipping normal fault, or a 75°-dipping strike-slip fault, we come to the following preliminary conclusion which await further detailed quantification:

- The influence of the near-field term on ground-motion intensities is very strong for dip-slip ruptures (normal fault and thrust-faulting), but less so for ruptures on near-vertical strike slip faults;
- The near-field terms are not equipartioned on the two horizontal component of motion, and hence need to be examined independently; they are also strongly developed on the vertical component, in particular for the dip-slip events on dipping fault;
- For thrust and normal-faulting events, the ground-motion intensities on the vertical component are particularly high; hence, any seismic hazard study concerned about the load on the building/structure due to vertically acting forces has to consider vertical motions for the radiated seismic wavefield;
- As the fault-dip becomes shallower, the symmetry of seismic radiation is broken more strongly, and near-field effects are more clearly distinguishable on the footwall and hanging wall sides of the fault;
- We do not find a significant effect of the velocity-density structure chosen in this study on the near-field terms and/or ground-motion intensities, most likely because none of the selected models is prone to surface-wave generation;
- The distance range in fault-normal direction over which the near-field effects are significant appears to depend on fault dip, in that for steeper dipping faults the range is smaller while the near-field effects are important over a wide region for shallowly dipping faults;
- Examining spectral acceleration at T = [1 2 3 5] sec and PGV, we do not find significant differences in the extent of the near-field region depending on period (or frequency of seismic waves), most likely due to finite-source effects that partially compensate the strict frequency effects of Eq. [3], but possible also because we consider a single magnitude and rise time only (hence limited the potentially radiated frequency spectrum);
- **Based on the shake maps, we conjecture that the spatial extent in fault-normal direction of the near-field affected area is related to fault width ($W$) and fault dip ($\delta$); a first-order estimate would be that this length scale is twice the surface-projection of the down-dip extent of the rupture, i.e.**

$$Y_{NF} = 2W \cdot \cos\delta \qquad \textbf{(4)}$$

- No conclusive statements are possible for the along-strike extent of the near-field affected area due to the limited domain size in our simulations;
- Realistic ground-motion simulations have to include near-field effects for any seismic hazard study that is concerned with ground-motion intensity measures (SA, PGV) that are sensitive to seismic waves at frequencies of 2 Hz and below.

## 1.8 Outlook

Our simulations for examining near-field and far-field effects establish the base reference cases against which refined numerical work could be carried out that includes more complex source models and a wider magnitude range. It is important to avoid a "contamination" of the spectral-response analysis of near-field terms by later arriving surface waves. This was partially achieved in this study, by avoiding near-surface shallow S-wave velocity layers. However, such layers are important contributors to ground motion complexity and site amplification, and hence should be included in a more comprehensive study on near-field effects. Moreover, refinement of this work requires a thorough analysis of the relative importance of near-field effect, depending on magnitude and source parameters (rupture speed, rise time, slip complexity). Finally, with a database of simulation results for many source models, faulting styles, and velocity models, one should attempt to develop an empirical relation that allows to estimate the "importance range" of near-field effects, based on source parameters (magnitude, distance, faulting style) and the frequency range of interest.

## 2. Relevance for DPC and/or for the scientific community

Since several factors, such as directivity and rise-time, cause ground shaking to be substantially different in the extreme NF than at larger distances, the knowledge of the NF/FF boundary is crucial. However, the computation of the entire wave-field in the low-frequency domain can have significant computation costs. In this work, we examine how to potentially derive empirical relations that may allow delineating NF/FF boundaries. If such a boundary can indeed be quantified, even if only approximately, one can choose to simulate ground-shaking for a given type of building or infrastructure, according to whether its location occurs in the NF or FF regime, with respect to a given source, and for a given frequency of interest.

## 3. Changes with respect to the original plans and reasons for it

We planed to derive a theoretical method for discriminating the important of near-field and far-field terms of seismic radiation. However, due to the nature of the problem, i.e. the complicated partitioning of the ground-shaking relevant S-wave energy in the near-field, intermediate-field and far-field seismic waves, we decided to develop empirical guidelines that can be closely linked to the DISS database. Our goal is achieved most efficiently by targeted numerical simulations that cover the parameter range of interest (source variability and source-site distance), considering also a set of earthquake rupture scenarios. In this work we focus on different faulting styles and a single magnitude, $M_w$ 7.1, the largest listed magnitude in the DISS database, as the near-field terms will become unimportant for smaller events. However, for $M_w$ 7.1 large ground-shaking and important near-field effects (including large static displacements) are expected, but the region over which these near-field effects dominate is not known. My thus concentrate our efforts to this single magnitude

As a potential extension, specific broadband simulations using the methodology described in Objective 1 could be performed. However, since the high-frequency contributions of such broadband simulations lack the detailed physics of the rupture process and the wave-propagation in the layered medium, such simulations would not help to examine the near-field boundary.

## 4. References

Aki, K., and Richards, P. G., 1980. Quantitative Seismology – Theory and Methods, Volume I and Volume II, ISBN 0-7167-1058-7(v.1), Copyright, 1980 by W.H. Freeman and Company.

Basili, R., Valensise, G., Vannoli, P., Burrato, P., Fracassi, U., Mariano, S., Tiberti, M. M., and Boschi, E., 2008. The Database of Individual Seismogenic Sources (DISS), version 3: summarizing 20 years of research on Italy's earthquake geology, Tectonophysics, doi:10.1016/j.tecto.2007.04.014

Graves, R., and A. Pitarka, 2004. Broadband time history simulation using a hybrid approach, 13th World Conference on Earthquake Engineering, Vancouver, B.C., Canada, August 1-6, 2004, paper number 1098.

Hole, J. A. (1992). Non-linear high resolution three-dimensional seismic travel time tomography, J. Geophys. Res., 97, 6553-6562

Ichinose, G.A., Goldstein, P., Rodgers, A.J., 2000. Relative importance of near, intermediate and far-field displacement terms in layered Earth synthetic seismogramsm. Bull. Seismol. Soc. Am. 90, 531–536.

Imperatori, W., and P.M. Mai (2009), Broadband Ground Motion Simulations in the Messina Strait Area (Southern Italy): Appraising Strong Motion Variability due to Complexity in Source and Earth Structure, manuscript in preparation

Madariaga, R. (2009). Earthquake source theory, in Treatise on Geophysics, Part 4 (Earthquake Seismology), Editors H. Kanamori and G. Schubert, Elsevier, pp.59-82.

Mai, M. P., and Beroza, G., 2003. A hybrid method for calculating near-source, broadband seismograms: application to strong motion prediction. Physics of the Earth and Planet. Int., 137: 183-199

Mai, P. M., Spudich, P., and Boatwright, J., 2005. Hypocenter locations in finite-source rupture models. Bull. Seis. Soc. Am, 95(3): 965-980.

Mai, P.M. (2009) Ground Motion: Complexity and Scaling in the Near Field of Earthquake Ruptures, in *Encyclopedia of Complexity and Systems Science*, W.H.K. Lee and R. Meyers (Eds.), Springer, *pp 4435-4474.*

Mai, P.M., W. Imperatori, K.B. Olsen (2010). Broadband ground motion simulations using finite-difference synthetics with local scattering operators, *in press for Bull. Seis. Soc. Am*.

Mena, B., P.M. Mai, K. B. Olsen, M. D. Purvance, and J. N. Brune (2010), Hybrid broadband ground motions simulation using scattering Greens functions: application to large magnitude events, in press Bull. Seis. Soc. Am.

Motazedian, D., Atkinson, G. M., 2005. Stochastic Finite-Fault Modeling Based on a Dynamic Corner Frequency. Bull. Seis. Soc. Am, 95(3): 995–1010.

Spudich, P., and Xu, L., 2003. Documentation of software package COMPSYN and ISOSYN sxv3.11. In: International Handbook of Earthquake and Engineering Seismology CD, IASPEI, Academic Press, 74 pp.

Wu, R.-S., and A. Ben-Menahem, 1985. The elasto-dynamic near-field, Geophys. J. R. astr. Soc, 81, 609-621.

Zonno, G., Musacchio, G., Basili, R., Imperatori, W., and Mai, P. M., 2008. Stochastic and full-wavefield finite-fault round-motion simulations of the M 7.1, Messina 1908 Earthquake (Southern Italy). Abstract presented at the A.G.U. Fall Meeting 2008, San Francisco (CA-USA), December 2008.

## 5. Key publications/presentation

*[following the completion of this deliverable]*